RSC Advances

PAPER

View Article Online
View Journal | View Issue

Cite this: *RSC Adv.*, 2025, **15**, 37570

Study on selective adsorption of organic pollutants in environmental water samples by solid-phase microextraction based on MOF-derived coatings

Junliang Du,[ab] Juan Li,[a] Ruiman Yin,[a] Shiyu Liu,[a] Ting Deng[a] and Xinzhen Du *[b]

Received 9th April 2025
Accepted 2nd October 2025

DOI: 10.1039/d5ra02456k

rsc.li/rsc-advances

A novel multifunctional coating strategy was developed through electrodeposition of $Co(OH)_2$ onto NiTi fibers, followed by *in situ* transformation into Zeolitic Imidazolate Framework-67(ZIF-67), and subsequent pyrolytic conversion under varied thermal conditions to yield three types of ZIF-67-derived coatings: (1) ZIF-67-Co_3O_4, (2) ZIF-67-nitrogen-doped carbon (ZIF-67-NC), and (3) ZIF-67-carbon (ZIF-67-C). The extraction selectivity of these coatings was systematically evaluated using HPLC-UV analysis against typical organic pollutants, including chlorinated pesticides (CPs), phthalate esters (PAEs), ultraviolet filters (UVFs), and polycyclic aromatic hydrocarbons (PAHs). Results demonstrated that the tailored pyrolytic treatments produced Co-based ZIF-67 derivatives with unique structural characteristics and selective adsorption properties: (i) ZIF-67-C exhibited superior specificity for PAHs adsorption, (ii) ZIF-67-NC demonstrated enhanced selectivity for UVFs extraction, and (iii) ZIF-67-Co_3O_4 displayed dual functionality for both PAHs and UVFs removal. This work not only elucidates the structure–property correlations in ZIF-67-based composites but also significantly expands the applicability of NiTi fibers in solid-phase microextraction (SPME) technology for environmental detection.

1 Introduction

With the development of industry and the increase of population, water pollution has emerged as one of the most critical environmental challenges.[1] A wide range of organic pollutants, including polycyclic aromatic hydrocarbons (PAHs), ultraviolet filters (UVFs), pesticides, and herbicides, have been detected in seawater, groundwater, and wastewater.[2] These contaminants exhibit high toxicity, persistent stability, and low biodegradability, posing significant risks such as carcinogenicity, mutagenicity, and endocrine disruption.[3] Consequently, the development of efficient, simple, and reliable methods for detecting organic pollutants in water has become imperative. However, most organic pollutants exist at trace or ultra-trace levels, rendering direct detection by conventional instruments impractical. Furthermore, environmental water samples are not homogeneous but comprise complex mixtures of various matrix components. The inherent characteristics of these samples-such as low target analyte concentrations, intricate matrices, abundant interferences, and susceptibility to environmental influences-have driven intensive research efforts into advancing sample pretreatment technologies.[4] To address these challenges, numerous sample pretreatment techniques have been developed. Traditional methods like solid-phase extraction (SPE) and liquid–liquid extraction (LLE) often require large quantities of highly toxic organic solvents and are associated with time-consuming and labor-intensive processes. In response, analytical chemistry has witnessed the evolution of solvent-free or low-solvent-consuming pretreatment methods. Among these, solid-phase microextraction (SPME), characterized by its solvent-free operation, reusability, and high adsorption efficiency, has gained widespread adoption in the determination of diverse analytes in environmental, food, pharmaceutical, biological, and clinical samples.[5–7]

SPME is based on the adsorption equilibrium between the target analytes in the sample solution and the fiber coating.[8] Therefore, its extraction performance is predominantly determined by the properties of the fiber coating,[9] particularly its chemical composition and morphological characteristics.[10] The compositional profile of the coating dictates the nature of intermolecular interactions with analytes, including but not limited to: π–π stacking interactions, hydrophobic/hydrophilic affinities, dipole–dipole coupling, electrostatic forces, hydrogen bonding interactions, These interaction modalities collectively determine the selectivity of the coating. The morphology of the coating dictates its specific surface area, which modulates the density of accessible interaction sites between the coating and target analytes. Enhanced specific surface area ffords greater binding site availability, leading to higher adsorption efficiency.[11,12]

[a]*College of Chemical and Materials Engineering, Mianyang Normal University, Mianyang, 621000, China*

[b]*College of Chemistry and Chemical Engineering, Northwest Normal University, Lanzhou, 730070, China. E-mail: fengzhongyundong@163.com*

In recent years, nanomaterials have gained increasing recognition for their potential in sample pretreatment technologies. Their high surface area offers abundant active sites for chemical reactions and physical exchanges necessary for target molecule adsorption. Additionally, nanomaterials exhibit short intraparticle diffusion distances, exceptional stability, superior reusability, and ease of fabrication and functionalization, all of which enhance their adsorption efficiency for specific analytes.[13] Moreover, the shape, size, and composition of nanostructures are key determinants of nanomaterial performance.[14,15] Consequently, the strategic development of novel nanocoatings with precisely tailored morphological and compositional architectures on fiber substrates has emerged as a robust methodological approach for the enhancement of both detection sensitivity and molecular selectivity in SPME detection.[8] Researchers have developed novel SPME nano coatings, including metal–organic frameworks (MOFs), layered double hydroxides (LDHs), molecularly imprinted polymers (MIPs), conductive polymers, carbon aerogels, covalent organic frameworks (COFs), and ionic liquids.[16–19] Among these materials, MOFs have garnered significant attention in SPME applications due to their feature-rich structures, high specific surface areas, and porosities, along with diverse metal coordination environments and functional groups.[20,21] However, practical challenges persist, particularly regarding the hydrothermal stability of MOFs, as water molecules can attack MOFs and induce framework collapse.[22] To mitigate this, MOF-derived materials (*e.g.*, carbon-based materials, metals, metal oxides, and their composites) have emerged as promising alternatives owing to their superior stability, porosity, and adsorption capacity.[23,24]

Initially, MOF-derived materials were incorporated into SPME using neutral silicone sealants as adhesives to immobilize them onto metal fiber substrates.[25–27] However, this approach reduces the effective surface area available for adsorption, compromising extraction efficiency. Subsequently, the Sol–Gel method was developed to enhance the stability and service life of coatings under high temperatures and organic solvents.[28] Nevertheless, this process requires multiple treatments to achieve the desired coating thickness, resulting in uneven thickness distribution and poor reproducibility across fibers. To overcome these limitations, the *in situ* synthesis of MOFs on fiber substrates followed by their *in situ* conversion into derivative materials has become a critical research focus for advancing MOF-derived SPME coatings.

Recently, MOFs materials have been successfully prepared *in situ* using metallic elements, metal oxides, or metal hydroxides as precursors.[29–32] Transforming metallic elements, metal oxides, or metal hydroxides into MOFs through an *in situ* conversion process, followed by pyrolysis to obtain MOF-derived materials, represents a rational approach to addressing the aforementioned challenges. As an adhesive-free preparation strategy, this method ensures the stability of the resulting coatings.

As a subclass of MOFs, ZIFs have been recognized as promising templates for the synthesis of composite materials. Previous research has demonstrated the *in situ* conversion of metallic coatings into ZIF-67 coatings, which were subsequently transformed into their derivative coatings for the enrichment of PAHs in environmental water samples.[33] However, studies on the *in situ* conversion of metal hydroxide materials into MOFs, followed by their transformation into derivative coatings for selective SPME of organic compounds, remain limited. In this study, $Co(OH)_2$ nanosheets were first electrodeposited onto NiTi fibers. Subsequently, $Co(OH)_2$ was *in situ* converted into ZIF-67 using 2-methylimidazole as the ligand. Finally, ZIF-67 was employed as a precursor to prepare different ZIF-67-derived composite coatings through pyrolysis under varying conditions: ① ZIF-67-Co_3O_4, ② ZIF-67-nitrogen-doped carbon (ZIF-67-NC), and ③ ZIF-67-carbon (ZIF-67-C) composite coatings. Using typical chlorinated pesticides (CPs), phthalate esters (PAEs), ultraviolet filters (UVFs), and polycyclic aromatic hydrocarbons (PAHs) as model analytes (the structures and property of the investigated aromatic compounds), the extraction selectivity of the composite coatings with different compositions was evaluated *via* high-performance liquid chromatography-ultraviolet detection (HPLC-UV). This work expands the application of NiTi fibers in SPME by leveraging the versatility of ZIF-67-derived materials.

2 Experimental

The details of the materials and reagents, instruments and preparation of sample solutions involved in this study are provided in the SI (SI).

2.1 Treatment of NiTi wires

The NiTi wires were treated according to a previously reported method.[34] Briefly, the NiTi wires were ultrasonically cleaned in acetone and ultrapure water for 10 minutes each. After cleaning, the wires were activated in a solution of HNO_3 and H_2O (1 : 1, v/v) for 30 minutes. Subsequently, the pretreated wires were immersed in a polytetrafluoroethylene-lined autoclave containing 2 mol L^{-1} NaOH solution and maintained in an oven at 110 °C for 10 hours. After hydrothermal treatment, the NiTi wires were rinsed with ultrapure water and air-dried, resulting in the preparation of NiTi@NiTiONFs fibers.

2.2 Electrochemical deposition of $Co(OH)_2$ coating on NiTi@NiTiONFs fibers

The $Co(OH)_2$ coating was electrochemically deposited on NiTi@NiTiONFs fibers according to a modified method.[35] Briefly, in a three-electrode system, the NiTi@NiTiONFs fiber, platinum wire, and saturated calomel electrode (SCE) were employed as the working electrode, counter electrode, and reference electrode, respectively. A $Co(NO_3)_2$ solution (0.05 mol L^{-1}) was used as the supporting electrolyte. A potential of −0.9 V was applied to the system at 40 °C for 1000 s. Subsequently, the resulting NiTi@NiTiONFs@$Co(OH)_2$ fibers were thoroughly rinsed to facilitate the subsequent *in situ* growth of ZIF-67.

2.3 *In Situ* growth of ZIF-67 on NiTi@NiTiONFs@$Co(OH)_2$ fibers

The *in situ* growth of ZIF-67 was carried out using a modified method.[23] Briefly, 2.46 g of 2-methylimidazole (2-MIM) was

placed in a sample bottle, followed by the addition of 7.5 mL of ultrapure water and 7.5 mL of ethanol. The mixture was ultrasonically dissolved to ensure homogeneity. Subsequently, the prepared NiTi@NiTiONFs@Co(OH)$_2$ fibers were threaded through the bottle cap and immersed in the above solution. The bottle was tightly sealed and placed in a 30 °C oil bath for 32 h. After the reaction, the resulting fibers were thoroughly washed with ethanol to remove residual 2-MIM. Finally, the fibers were dried in an oven at 60 °C for 6 h, followed by further drying at 100 °C for 12 h, yielding the NiTi@NiTiONFs@ZIF-67 fibers.

2.4 *In situ* transformation of ZIF-67 into ZIF-67-derived coatings

The *in situ* transformation of ZIF-67 into its derived materials was conducted based on an improved method.[33] The prepared NiTi@NiTiONFs@ZIF-67 fibers were subjected to different thermal treatments under controlled conditions. For the synthesis of NiTi@NiTiONFs@ZIF-67-Co_3O_4 fibers, the fibers were heated under a nitrogen (N_2) atmosphere at a ramp rate of 2 °C min^{-1} to 350 °C, followed by maintaining the temperature at 350 °C for 2 h, and subsequently cooled to room temperature. To obtain NiTi@NiTiONFs@ZIF-67-NC fibers, the fibers were heated under a nitrogen (N_2) atmosphere at a ramp rate of 2 °C min^{-1} to 250 °C, held at 250 °C for 1 h, and then cooled to room temperature. For the preparation of NiTi@NiTiONFs@ZIF-67-C fibers, the fibers were heated under vacuum at a ramp rate of 2 °C min^{-1} to 250 °C, maintained at 250 °C for 1 h, and finally cooled to room temperature. These thermal treatments facilitated the controlled transformation of ZIF-67 into its respective derivatives, yielding functionalized fibers with tailored properties.

2.5 SPME-HPLC procedure

The SPME-HPLC process was conducted as follows: 15 mL of the standard solution was placed in a 20 mL sample vial. Sodium chloride (NaCl) was added to control the ionic strength of the solution, and a phosphate buffer was used to adjust the pH value. The prepared fiber was then immersed into the sample vial and stirred in the solution at a predetermined temperature for a specified period. After extraction, the fiber was promptly removed and inserted into the SPME-LC interface for static desorption using the mobile phase. Subsequently, HPLC analysis was performed. For the detection of polycyclic aromatic hydrocarbons (PAHs), chlorophenols (CPs), phthalate esters (PAEs), and ultraviolet filters (UVFs), the mobile phase compositions (methanol/water, v/v) were set to 85/15, 70/30, 75/25, and 85/15, respectively. The detection wavelengths were 254 nm, 282 nm, 280 nm, and 310 nm for PAHs, CPs, PAEs, and UVFs, respectively. After each extraction, the fiber was rinsed sequentially with methanol and ultrapure water for 5 min each to eliminate potential residual effects and ensure reproducibility.

3 Results and discussion

3.1 Characterization of NiTi@NiTiONFs fibers

As shown in Fig. 1a and b, the surface of the bare NiTi wire is smooth but exhibits cracks. Based on the elemental

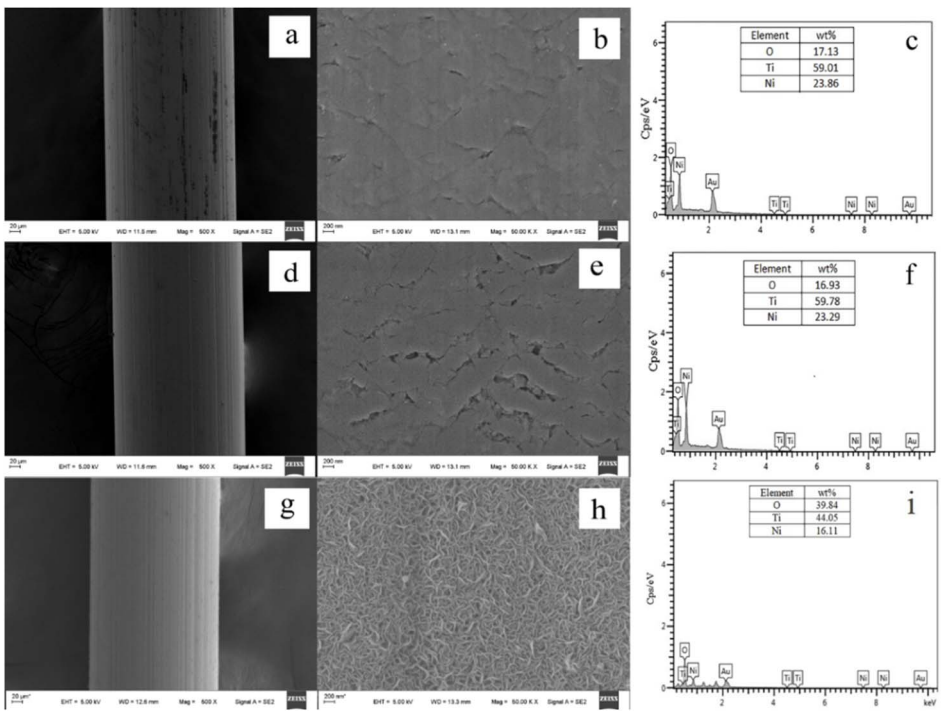

Fig. 1 Low- and high-magnification SEM images and EDS spectra of different fibers (a)–(c) bare NiTi wire; (d)–(f) pretreated NiTi wire; (g)–(i) hydrothermally treated NiTi wire.

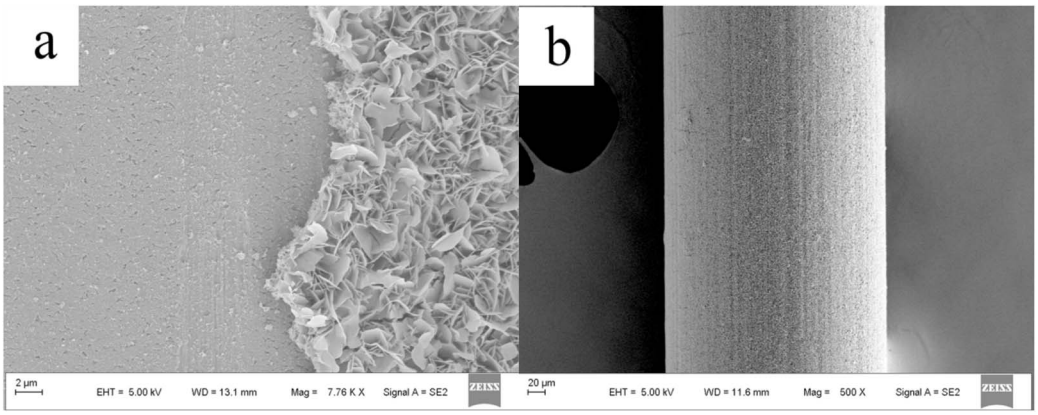

Fig. 2 SEM images of $Co(OH)_2$ electrodeposited on different substrates (a) direct electrodeposition of $Co(OH)_2$ coating on the bare NiTi wire; (b) electrodeposition of $Co(OH)_2$ coating on the fiber after hydrothermal treatment with NaOH.

composition of Ni, Ti, and O (Fig. 1c), it is evident that the surface is covered with a composite oxide passivation layer. From Fig. 1d–f, it can be observed that after acid treatment, the morphology and the content of Ni, Ti, and O elements remain largely unchanged, indicating the excellent corrosion resistance of the commercial NiTi wire. Fig. 1g and h reveal that after hydrothermal treatment of the NiTi wire in a NaOH solution, a uniform nanosheet-like structure is grown on the NiTi fiber substrate. The surface of the resulting nanosheet coating is also composed of Ni, Ti, and O elements, but the atomic percentage of O is significantly increased. This suggests that the newly grown TiO_2 and NiO composite coating (NiTiONFs) has replaced the original passivation layer, denoted as NiTi@NiTiONFs fibers. In comparison to the direct electrodeposition of $Co(OH)_2$ coating on the bare NiTi wire (Fig. 2a), the electrodeposition of $Co(OH)_2$ coating on the fiber after NaOH

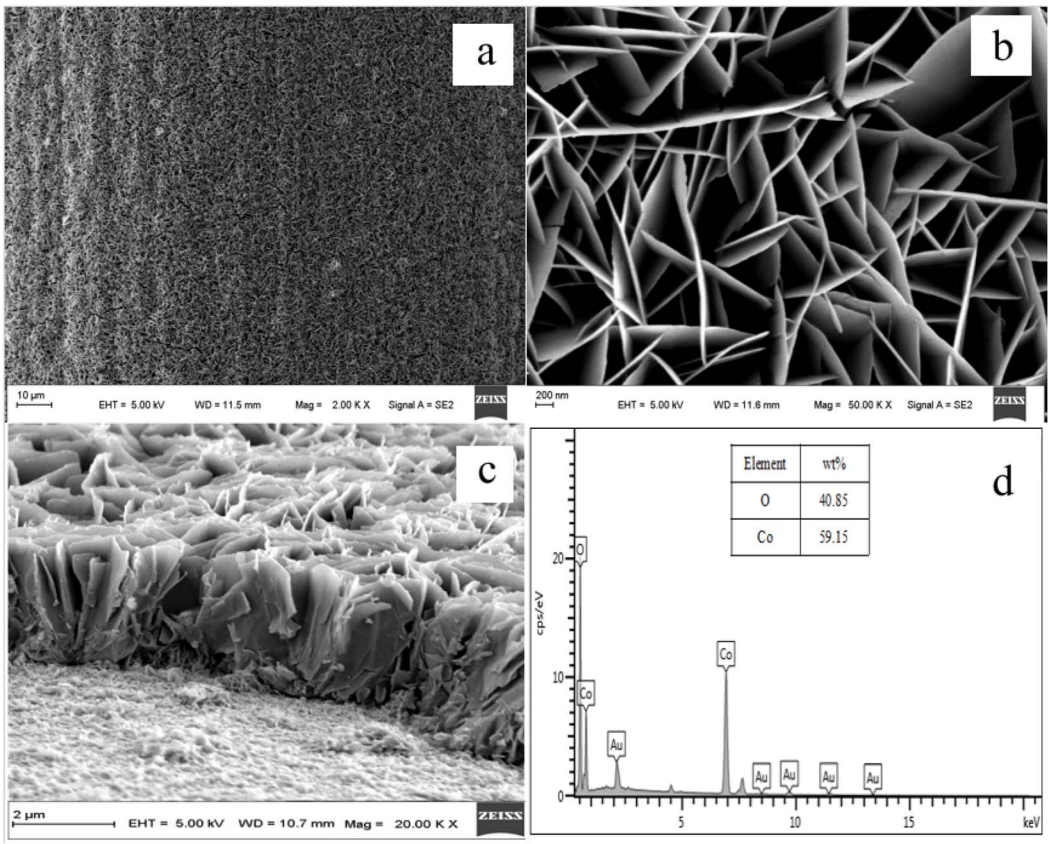

Fig. 3 SEM and EDS images of $Co(OH)_2$ (a) low-magnification SEM image; (b) high-magnification SEM image; (c) cross-sectional image; (d) EDS spectrum.

hydrothermal treatment is uniform and robust (Fig. 2b). Therefore, the NiTi@NiTiONFs fibers obtained after NaOH hydrothermal treatment were employed as the fiber substrate for subsequent investigations.

3.2 Characterization of NiTi@NiTiONFs@$Co(OH)_2$ fibers

The morphology of the obtained NiTi@NiTiONFs@$Co(OH)_2$ fibers was investigated using scanning electron microscopy (SEM). Fig. 3a and b present low- and high-magnification SEM images of the fibers, revealing a uniform coverage of two-dimensional (2D) nanosheets on the fiber surface. The coating consists of interconnected nanosheets with a thickness of approximately 10 nm. This ordered structure is expected to exhibit a high specific surface area, which can enhance the extraction efficiency in solid-phase microextraction (SPME). Additionally, the cross-section of the fiber was analyzed by SEM, as shown in Fig. 3c. It is evident that the nanosheets are vertically aligned on the substrate surface, forming a porous nanowall structure with high porosity. This phenomenon is attributed to the CdI_2-type layered structure of $Co(OH)_2$, which features weak interlayer interactions and strong intralayer bonding. Consequently, $Co(OH)_2$ preferentially grows along the layered planes, resulting in the formation of 2D nanosheet structures.[36] To further confirm the chemical composition of the obtained nanosheets, energy-dispersive X-ray spectroscopy (EDS) analysis was conducted. As depicted in Fig. 3d, the coating contains Co and O elements with an atomic ratio of approximately 1 : 2. Based on literature review, the following reactions occur when $Co(NO_3)_2$ is used as the electrolyte: $NO_3^- + 7H_2O + 8e^- = NH_4^+ + 10OH^-$ and $Co_2^+ + 2OH^- = Co(OH)_2$.[37] Therefore, the resulting coating is confirmed to be composed of $Co(OH)_2$ nanosheets.

3.3 Characterization of NiTi@NiTiONFs@$Co(OH)_2$@ZIF-67 fibers

In the NiTi@NiTiONFs@$Co(OH)_2$ fibers, the $Co(OH)_2$ coating on the surface serves as a self-sacrificial template, providing Co^{2+} ions that coordinate with 2-methylimidazole (2-MIM) in the solution to enable the *in situ* growth of a ZIF-67 coating. This process occurs because the 2-MIM ligands undergo deprotonation to generate H^+ ions, which react with $Co(OH)_2$ to release Co^{2+} ions. The released Co^{2+} ions diffuse outward and coordinate with 2-MIM on the outer surface of $Co(OH)_2$, leading to the *in situ* crystallization of ZIF-67. During the synthesis of ZIF-67, 2-MIM plays a dual role: it acts as both an etchant to release Co^{2+} ions and a coordinating agent for Co^{2+} ions.[35,38] Fig. 4 shows the SEM and EDS images of the NiTi@NiTiONFs@$Co(OH)_2$@ZIF-67 fibers. As depicted in the images, the fiber surface is uniformly covered with dodecahedral nanomaterials (Fig. 4a–c). The corresponding surface elemental composition was analyzed using EDS (Fig. 4d). The results indicate that the atomic percentages of carbon, nitrogen, and cobalt are 49.72%, 20.34%, and 29.94%, respectively, which is highly consistent with previous studies,[17] confirming that the coating is ZIF-67.

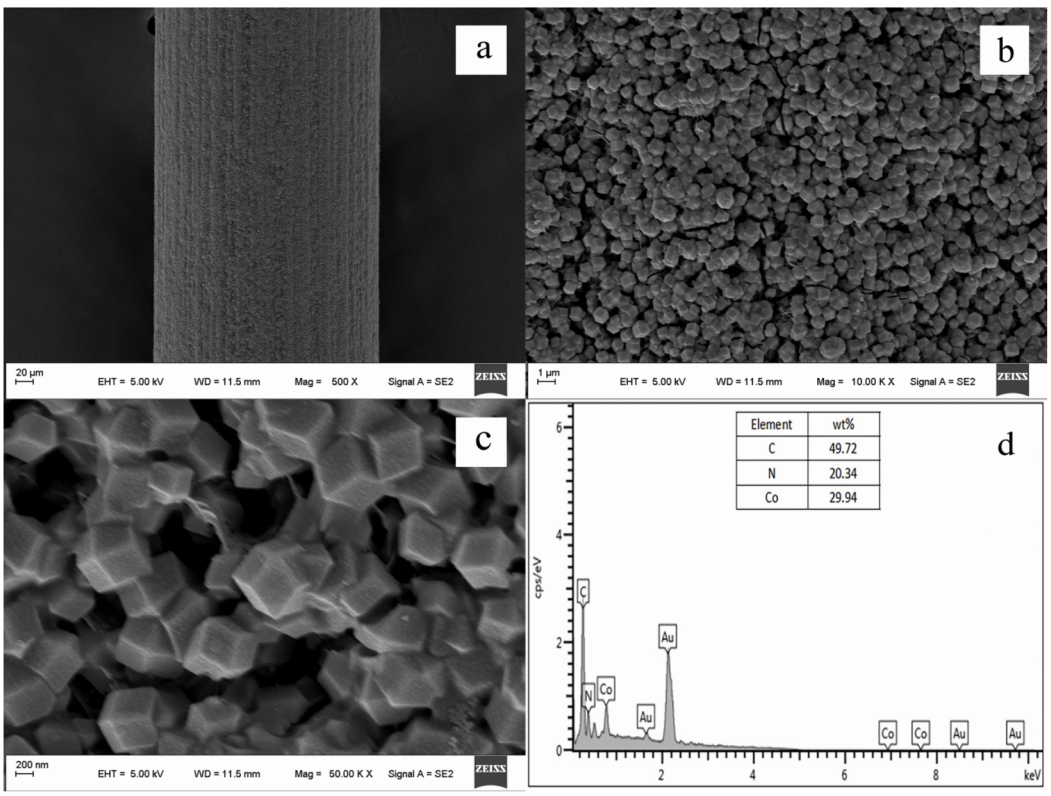

Fig. 4 SEM images (a–c) and EDS spectrum (d) of the ZIF-67 coating.

3.4 Characterization of NiTi@NiTiONFs@ZIF-X (X = Co_3O_4, C, and NC) fibers

The fibers were subjected to low-temperature pyrolysis under nitrogen (N_2) and vacuum conditions to obtain ZIF-Co_3O_4, ZIF-C, and ZIF-NC coatings, respectively. The morphological features and corresponding elemental compositions were investigated using SEM and EDS. Fig. 5a and d show the SEM and EDS images of the ZIF-Co_3O_4 coating prepared by heating the fiber in N_2 at a ramp rate of 2 °C min^{-1} from room temperature to 350 °C, maintaining the temperature at 350 °C for 2 h, and then cooling to room temperature. The elemental analysis from the EDS spectrum (Fig. 5d) reveals an atomic ratio of Co to O of 3 : 4, confirming the formation of a Co_3O_4 coating. As shown in Fig. 5a, compared to the original dodecahedral shape of ZIF-67, the ZIF-67-derived Co_3O_4 exhibits significant shrinkage and the presence of cracks after the annealing process. This phenomenon is attributed to the substantial shrinkage of the coating during sintering, while the substrate dimensions remain unchanged at the sintering temperature. The mismatch in the thermal expansion coefficients between the coating and the substrate leads to crack formation during sintering. These additional cracks increase the exposure of active sites, thereby enhancing adsorption efficiency. Fig. 5b and e present the SEM and EDS images of the ZIF-C coating obtained by heating the fiber under vacuum at a ramp rate of 2 °C min^{-1} to 250 °C, maintaining the temperature at 250 °C for 1 h, and then cooling to room temperature. The EDS spectrum (Fig. 5e) indicates that the ZIF-C coating contains carbon, oxygen, and cobalt with mass fractions of 24.16%, 18.47%, and 57.36%, respectively, suggesting that the coating is a composite of CoO and carbon. As shown in Fig. 5b, the ZIF-C coating retains the overall morphology of ZIF-67 but exhibits some shrinkage and the presence of cracks.

Fig. 5c and f display the SEM and EDS images of the ZIF-NC coating prepared by heating the fiber in N_2 at a ramp rate of 2 °C min^{-1} from room temperature to 250 °C, maintaining the temperature at 250 °C for 1 h, and then cooling to room temperature. The EDS spectrum (Fig. 5f) reveals the coexistence of carbon, nitrogen, oxygen, and cobalt in the coating, with mass fractions of 51.06%, 10.02%, 11.80%, and 27.11%, respectively, indicating that the coating is a composite of CoO and nitrogen-doped carbon (NC). As shown in Fig. 5c, compared to the ZIF-67 coating, the ZIF-NC coating exhibits uniform shrinkage, relatively consistent dimensions, and a rough surface.

3.5 Extraction selectivity

Studies have demonstrated that the adsorption efficiency of adsorbents is predominantly determined by the surface area of the coating, which is closely related to its morphology.[39] Specifically, the morphology of the coating significantly influences its extraction performance, while the selectivity of the coating is governed by its chemical composition.[22] For instance, metal oxide coatings exhibit a high affinity for aromatic compounds due to the cation-π interactions between metal cations on the oxide surface and aromatic molecules.[40] Furthermore, carbon materials doped with heteroatoms, such as metals (M), metal oxides (MO), and other non-metallic elements (*e.g.*, N, O, B, S), can substantially enhance the performance of carbon-based materials. Carbon materials doped with heteroatoms, particularly nitrogen, exhibit exceptional capabilities in adsorbing organic compounds.[22] Owing to their high porosity, surface functionality, and hydrophobicity, carbon-based materials have become one of the most extensively studied adsorbents for the purification of wastewater, especially for aromatic compounds.[40] To investigate the extraction selectivity and capacity of the prepared carbon-based

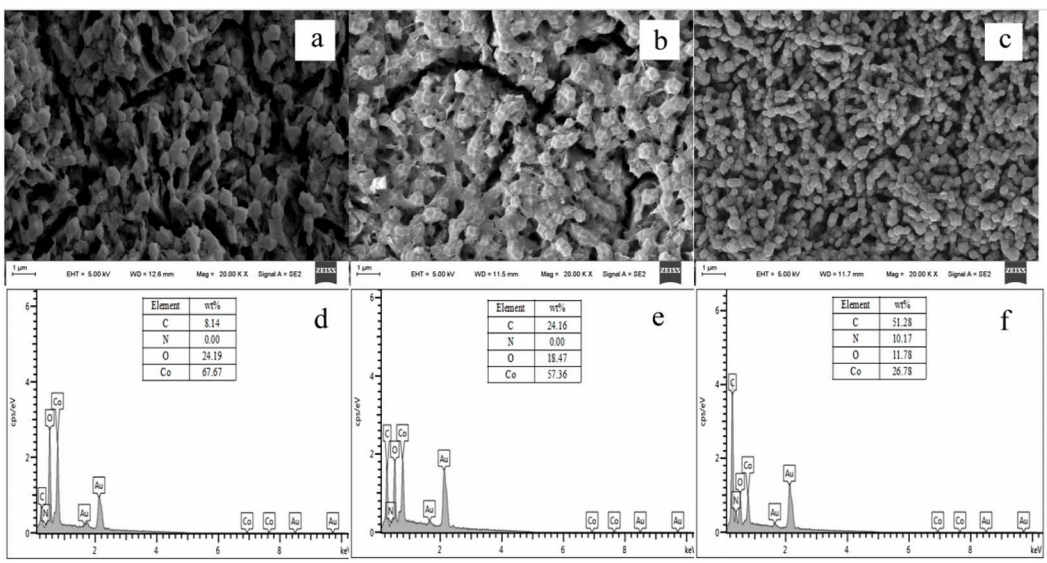

Fig. 5 SEM images (a–c) and EDS spectra with corresponding elemental compositions (d–f) of the ZIF-X (X = Co_3O_4 (a and d), C (b and e), and NC (c and f)) coatings.

coatings, four groups of typical aromatic compounds with distinct molecular structures-chlorophenols (CPs), phthalate esters (PAEs), ultraviolet filters (UVFs), and polycyclic aromatic hydrocarbons (PAHs)-were selected as model analytes.

Fig. 6 illustrates the adsorption selectivity of NiTi@NiTiONFs/ZIF-X (X = Co_3O_4 (Fig. 6a), C (Fig. 6b), and NC (Fig. 6c)) fibers for four typical aromatic compounds. From the data presented, it is observed that the NiTi@NiTiONFs@ZIF-67-Co_3O_4 fiber exhibits comparable extraction capabilities for UVFs and PAHs (Fig. 6a). In contrast, the NiTi@NiTiONFs@ZIF-67-C fiber demonstrates a lower extraction efficiency for UVFs compared to PAHs (Fig. 6b). This phenomenon may be attributed to the π-electron interactions between the aromatic rings of polycyclic aromatic hydrocarbons (PAHs) and the sp^2 graphitic carbon planes of the carbon material. Furthermore, the incorporation of carbon elements enhances the hydrophobicity of the coating, thereby improving its adsorption selectivity toward PAHs.[41] Therefore, the hydrophobic interaction, cation-π interactions and the π–π interaction between PAHs and the Co–C coating collectively contribute to the superior adsorption capacity of the NiTi@NiTiONFs @ZIF-67-C fiber for PAHs.[42] Conversely, the NiTi@NiTiONFs@ZIF-67-NC fiber shows a higher extraction efficiency for UVFs than for PAHs (Fig. 6c). Increasing evidence suggests that the doping of heteroatoms (*e.g.*, N, B, S, and P) in carbon materials significantly influences their electrochemical and physical properties. Such doping can effectively maintain the robust framework and intrinsic structural characteristics of nanostructured carbon while enhancing its performance. Notably, nitrogen doping has a more pronounced impact on altering the properties of carbon compared to other heteroatoms.[43] This is because nitrogen-containing groups increase the basicity of the carbon surface, creating polar sites capable of binding polar molecules. As reported by Lorenc-Grabowska *et al.*[44] the polarity increases with higher nitrogen content, *N*-doping can modify the elemental composition of the coatings and tailor the hydrophilicity and hydrophobicity of the coatings.[42] Consequently, the NiTi@NiTiONFs@ZIF-67-NC fiber exhibits stronger hydrophilicity compared to the NiTi@NiTiONFs@ZIF-67-C fiber, resulting in superior adsorption performance for UVFs. Additionally, Fig. 6 reveals that all ZIF-67-derived coatings exhibit negligible extraction capabilities for hydrophilic CPs and PAEs. This result indicates that the composition of the coating significantly influences extraction selectivity. Therefore, the *in situ* prepared NiTi@NiTiONFs@ZIF-67-C fiber can be considered a potential candidate for extracting PAHs, while the NiTi@NiTiONFs@ZIF-67-NC fiber is a promising candidate for extracting UVFs.

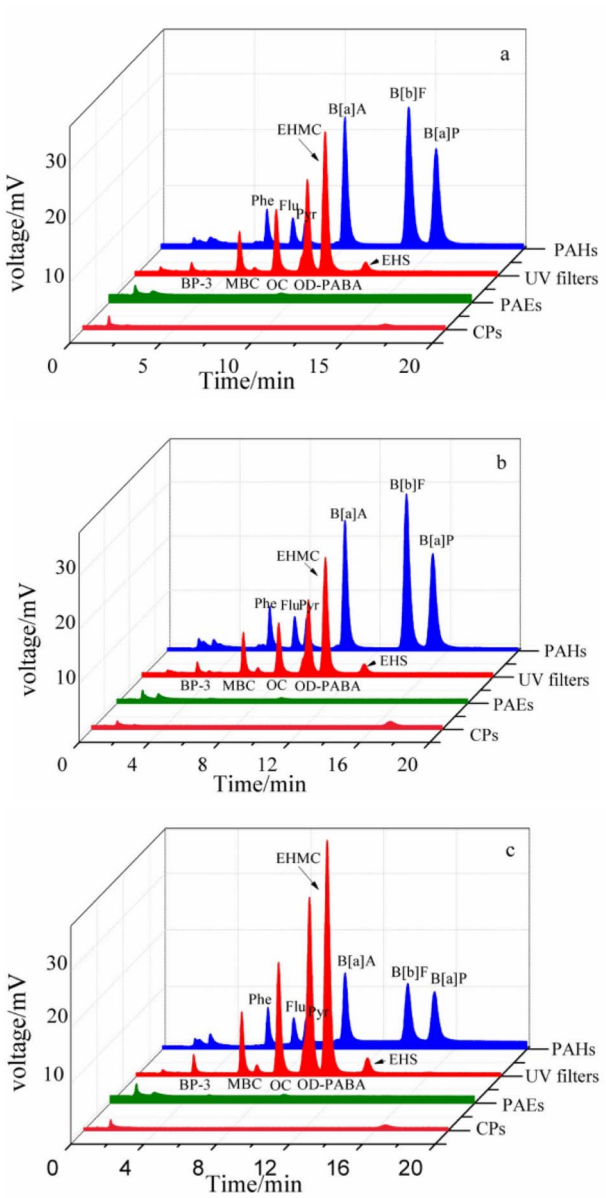

Fig. 6 SPME-HPLC chromatograms of (a) NiTi@NiTiONFs@ZIF-67-Co_3O_4, (b) NiTi@NiTiONFs@ZIF-67-C, and (c) NiTi@NiTiONFs@ZIF-67-NC.

Consequently, the carbon doping enhances the hydrophobicity of the coating, while nitrogen doping increases its hydrophilicity, thereby modifying the adsorption selectivity of the fiber. The strategic incorporation of doped coatings enables precise tuning of sorptive properties, as demonstrated by previous studies: The Qian research group achieved significant performance enhancement through the synthesis of Cu-MOF-doped poly(vinylidene fluoride-*co*-hexafluoropropylene) (PVDF-HFP) on polyethylene terephthalate (PET) fibers.[45] The Szekely research group developed nanofiber membranes comprising intrinsically microporous polyimide-doped MOFs for volatile organic compound (VOC) capture.[46]

3.6 Stability and reusability of the fabricated fibers

To verify the stability and reusability of the prepared fibers, this study investigated their cycling performance as well as their stability and robustness after prolonged use. The results demonstrated that No significant decrease in peak areas was observed even after 100 cycles of extraction and desorption, The recoveries from 91.2% to 93.6% were achieved for spiking water at the level of 100 μg L^{-1}, indicating that the fabricated fibers presents excellent reusability. Meanwhile, Fig. S1 presents comparative SEM and EDS analyses of the as-fabricated coating

before and after 100 extraction–desorption cycles, revealing negligible alterations in both morphological features and elemental composition, which conclusively demonstrates its long-term stability and robustness.

4 Conclusions

Following the electrodeposition of a $Co(OH)_2$ coating on the hydrothermally treated NiTi fiber substrate, ZIF-67 was grown *in situ* and subsequently transformed into different ZIF-67-derived coatings through controlled thermal treatments. The diverse processing methods yielded coatings with distinct compositions, which significantly influenced their extraction selectivity. The ZIF-67-Co_3O_4 coating demonstrated high extraction capabilities for both PAHs and UVFs but lacked selectivity. In contrast, the ZIF-67-C coating exhibited selective adsorption for PAHs, while the ZIF-67-NC coating showed selective extraction for UVFs. Consequently, the NiTi@NiTiONFs@ ZIF-67-C fiber emerges as a potential candidate for extracting PAHs, and the NiTi@NiTiONFs@ZIF-67-NC fiber is a promising candidate for extracting UVFs. This novel *in situ* transformation strategy expands the potential applications of NiTi fibers in solid-phase microextraction (SPME), offering a versatile approach to tailoring fiber coatings for selective extraction of target analytes.

Conflicts of interest

There are no conflicts to declare.

Data availability

All datas of this study are avalilable within the paper and its Supplement Information (SI). Supplementary information is available. See DOI: **https://doi.org/10.1039/d5ra02456k**.

Acknowledgements

This project was financially supported by the Scientific Research Fund of Mianyang normal university (QD2021A36).

References

1 Y. Y. Yang, H. P. Feng, X. G. Zhang, H. Guo, X. J. Wen, L. Sui, Z. T. Dong, M. Yan and C. G. Niu, *Chem. Eng. J.*, 2024, **490**, 151309.
2 I. W. Rushdi, R. Hardian, R. S. Rusidi, W. M. Khairul, S. Hamzah, W. M. A. Khalik, N. S. Abdullah, N. K. E. M. Yahaya, G. Szekely and A. A. A. Che, *Eng. J.*, 2025, **510**, 161595.
3 M. Rio, G. T. Palomino and C. P. Cabello, *ACS Appl. Mater. Interfaces*, 2020, **12**, 6419–6425.
4 H. L. Jiang, N. Li, L. Cui, X. Wang and R. S. Zhao, *TrAC, Trends Anal. Chem.*, 2019, **120**, 115632.
5 M. Llompart, M. Celeiro, C. García-Jares and T. Dagnac, *TrAC, Trends Anal. Chem.*, 2019, **112**, 1–12.
6 C. H. Xu, G. S. Chen, Z. H. Xiong, Y. X. Fan, X. C. Wang and Y. Liu, *TrAC, Trends Anal. Chem.*, 2016, **80**, 12–29.
7 N. Reyes-Garcés and E. Gionfriddo, *TrAC, Trends Anal. Chem.*, 2019, **113**, 172–181.
8 V. Jalilia, A. Barkhordarib and A. Ghiasvand, *Microchem. J.*, 2020, **152**, 104319.
9 M. D. F. Alpendurada, *J. Chromatogr. A*, 2000, **889**, 3–14.
10 E. A. S. Silva, S. Risticevic and J. Pawliszyn, *TrAC, Trends Anal. Chem.*, 2013, **43**, 24–36.
11 Y. K. Xiong, P. Du, S. J. Huang, S. F. He, X. Li, J. Yang and Y. Yang, *ACS Appl. Polym. Mater.*, 2024, **6**, 5674–5683.
12 J. Zheng, J. L. Huang, Q. Yang, C. Y. Ni, X. T. Xie, Y. R. Shi, J. F. Sun, F. Zhu and G. F. Ouyang, *TrAC, Trends Anal. Chem.*, 2018, **108**, 135–153.
13 P. K. Gautam, A. Singh, K. Misra, A. K. Sahoo and S. K. Samanta, *J. Environ. Manage.*, 2019, **231**, 734–748.
14 Y. N. Ou, G. R. Li, Z. L. Wang, X. L. Yu and Y. X. Tong, *J. Electrochem. Soc.*, 2010, **157**, 264–268.
15 S. F. Huang, C. W. Tung, T. S. Chan and H. M. Chen, *CrystEngComm*, 2016, **18**, 6008–6012.
16 J. Zheng, J. L. Huang, Q. Yang, C. Y. Ni, X. T. Xie, Y. R. Shi, J. F. Sun, F. Zhu and G. F. Ouyang, *TrAC, Trends Anal. Chem.*, 2018, **108**, 135–153.
17 M. Lashgari and Y. Yamini, *Talanta*, 2019, **191**, 283–306.
18 X. M. Yang, J. M. Wang, W. J. Wang, S. H. Zhang, C. Wang, J. H. Zhou and Z. Wang, *Microchim. Acta*, 2019, **186**, 145.
19 X. M. Yang, S. H. Zhang, J. M. Wang, W. J. Wang, J. Q. Li, J. W. Chen, Y. J. Zhao, C. Wang and Z. Wang, *Anal. Chim. Acta*, 2020, **1134**, 50–57.
20 Y. Wang, M. Rui and G. Lu, *J. Sep. Sci.*, 2018, **41**, 180–194.
21 P. Rocío-Bautista, I. Pacheco-Fernández, J. Pasán and P. Verónica, *Anal. Chim. Acta*, 2016, **939**, 6–41.
22 Q. K. Hu, S. Q. Liu, X. Chen, J. Q. Xu, F. Zhu and G. F. Ouyang, *Anal. Chim. Acta*, 2019, **1047**, 1–8.
23 G. R. Cai, W. Zhang, L. Jiao, S. H. Yu and H. L. Jiang, *Chem*, 2017, **2**, 791–802.
24 B. N. Bhadra, A. Vinu, C. Serre and S. H. Jhung, *Mater. Today*, 2019, **25**, 88–111.
25 S. H. Zhang, Q. Yang, Z. Li, W. C. Wang, C. Wang and Z. Wang, *Analyst*, 2016, **141**, 1127–1135.
26 S. H. Zhang, Q. Yang, X. Yang, W. C. Wang, Z. Li, L. H. Zhang, C. Wang and Z. Wang, *Talanta*, 2017, **166**, 46–53.
27 X. R. Hu, C. H. Wang, J. S. Li, R. Luo, C. Liu, X. Y. Sun, J. Y. Shen, W. Q. Han and L. J. Wang, *ACS Appl. Mater. Interfaces*, 2018, **10**, 15051–15057.
28 X. Zhang, X. H. Zang, J. T. Wang, C. Wang, Q. H. Wu and Z. Wang, *Microchim. Acta*, 2015, **182**, 2353–2359.
29 X. Y. Cui, Z. Y. Gu, D. Q. Jiang, Y. Li, H. F. Wang and X. P. Yan, *Anal. Chem.*, 2009, **81**, 9771–9777.
30 F. X. Wei, Y. H. He, X. L. Qu, Z. Y. Xu, S. R. Zhang, D. Q. Zhu and H. Y. Fu, *Anal. Chim. Acta*, 2019, **1078**, 70–77.
31 S. T. Sun, L. J. Huang, H. Y. Xiao, Q. Shuai and S. H. Hu, *Talanta*, 2019, **202**, 145–151.
32 X. Ling and Z. L. Chen, *Talanta*, 2019, **192**, 142–146.
33 J. L. Du, R. Zhang, F. F. Wang, X. M. Wang and X. Z. Du, *J. Chromatogr. A*, 2020, **118**, 460855.
34 H. J. Wang, W. L. Song, M. Zhang, Q. Zhen, M. Guo, Y. D. Zhang and X. Z. Du, *J. Chromatogr. A*, 2016, **1468**, 33–41.

35 Z. L. Chen, Y. Ha, H. X. Jia, X. X. Yan, M. Chen, M. LIu and R. B. Wu, *Adv. Energy Mater.*, 2019, **9**, 1803918.
36 J. B. Wu, Y. Lin, X. H. Xia, J. Y. Xu and Q. Y. Shi, *Electrochim. Acta*, 2011, **56**, 7163–7170.
37 C. Z. Yuan, L. Yang, L. R. Hou, L. F. Shen, X. G. Zhang and X. W. Lou, *Energy Environ. Sci.*, 2012, **5**, 7883–7888.
38 M. C. Guo, Y. Li, L. X. Zhou, Q. J. Zheng, W. J. Jie, F. Y. Xie, C. G. Xu and D. M. Lin, *Electrochim. Acta*, 2019, **298**, 525–532.
39 B. N. Bhadra, J. Y. Song, S. K. Lee, Y. K. Hwang and S. H. Jhung, *J. Hazard. Mater.*, 2018, **344**, 1069–1077.
40 J. Xu, P. Wu, E. C. Ye, B. F. Yuan and Y. Q. Feng, *TrAC, Trends Anal. Chem.*, 2016, **80**, 41–56.
41 M. J. Yuan, S. T. Tong, S. Q. Zhao and C. Q. Jia, *J. Hazard. Mater.*, 2010, **181**, 1115–1120.
42 J. L. Du, R. Zhang, F. F. Wang, H. Zhou, X. M. Wang and X. Z. Du, *Chin. Chem. Lett.*, 2022, **33**, 3119–3122.
43 Q. Li, H. Y. Pan, D. Higgins, R. G. Cao, G. Q. Zhang, H. F. Lv, K. B. Wu, J. Cao and G. Wu, *Small*, 2015, **11**, 1443–1452.
44 E. Lorenc-Grabowska, G. Gryglewicz and J. Machnikowski, *Appl. Surf. Sci.*, 2010, **256**, 4480–4487.
45 M. Hong, X. Ma, W. Y. Hu, C. Zhu, W. Dong, L. M. Chen and F. P. Qian, *Sep. Purif. Technol.*, 2025, **362**, 131725.
46 F. Topuz, M. A. Abdulhamid, R. Hardian, T. Holtzl and G. Szekely, *J. Hazard. Mater.*, 2022, **424**, 127347.